Calculation of Differential-Turning Barrier Surfaces

Henry J. Kelley* and Leon Lefton†
Analytical Mechanics Associates, Inc., Jericho, New York

The computation of composite differential-turn trajectory pairs is studied for "fast-evader" and "neutral-evader" idealizations introduced in earlier publications. Transversality and generalized corner conditions are examined and the joining of trajectory segments discussed. A criterion is given for the screening of "tandem-motion" trajectory segments. Main focus is upon the computation of barrier surfaces. Fortunately, from a computational viewpoint, the trajectory pairs defining these surfaces need not be calculated completely, the final subarc of multiple-subarc pairs not being required. Weapon effects are introduced in terms of generally forward-firing but trainable weapons whose envelopes are described by radius limits and conic trainability limits. The pursuer may elect to fill a turn-angle gap with his weaponry, while meeting the usual energy-matching requirement, or he may choose instead to close angularly to tail-chase position, relying on the weapon's upward reach to compensate for an energy deficiency; most often the choice will be intermediate between these extremes. In some cases, dissimilarities in flight performance characteristics between the opposing aircraft tend to favor the pursuit tactic of closing angularly, then driving the evader aloft for an energy-attrition duel, and generally the upward reach of the weaponry increases the effectiveness of such a tactic, permitting its use with relatively low pursuer energy. Illustrative computations are presented for various pairs of example aircraft.

Introduction

THE modeling of a turning chase in air combat as a differential game with energy-modeled vehicles is described in Ref. 1 and the characteristics of families of solutions are investigated in Ref. 2. The present paper, a sequel, deals with the computational solutions of families, with emphasis upon the determination of barrier surfaces, those surfaces that, when closed, separate successful pursuit from successful evasion. It will be assumed, for brevity, to be read in conjunction with Refs. 1 and 2.

The studies of Refs. 1 and 2 employ the rough equivalent of a point-capture criterion, viz. the pursuer must overtake the evader in turn angle while possessing sufficient specific energy to follow in a pull up. This last requirement is expressed in energy approximation in terms of equaling or exceeding the evader's loft-ceiling, the highest altitude at which the craft can attain vertical equilibrium at the specific energy. This capture criterion is recommended by its simplicity for the purpose of development of computational technique and for exploratory applications work, and it will be used in the bulk of the computational results to be presented. However, a first step will be taken to bring in weapon-envelope effects in terms of a simple form of envelope, expressed by a radius limit and conic trainability limit, in some of the results.

Transversality Conditions: "Fast-Evader" Model

A simplified version of the problem is of interest initially for illustrative purposes. Thus attention is directed to the "fast-evader" altitude-dynamics idealization, in which both pursuer and evader have a free choice of altitude within their respective bounds and no intervals of "tandem motion," with the pursuer driving the evader upward, appear.[2]

Consideration of a related problem with vehicle models further reduced in order[2] suggests that fast-evader trajectory pairs have the following form. For the aircraft having the higher maximum sustainable turn rate as *evader,* there is simple pairing of Euler solutions terminating in the "capture set," a subset of the "target set" (both defined in Ref. 1) or on its boundary. If the sustainable-turn-rate-superior aircraft is pursuer, and if it is inferior to the evader in maximum instantaneous turn rate, some of the trajectory pairs have two subarcs. The initial subarc almost attains turn-angle closure with loft-ceiling-matched energies; the second comprises a high-turn-rate pair of trajectories joined to the first at a corner and terminates in the capture set or on its boundary.

If the capture set lies entirely above the loft-ceiling-match curve in energy space (pursuer specific energy chosen as the ordinate), capture necessarily takes place with the loft-ceiling inequality met with a margin, and both energy multiplier variables vanish at the final point by transversality. Such a situation arises in the case just mentioned exhibiting evader superiority in maximum instantaneous turn rate at matched loft-ceilings, as in Fig. 7 of Ref. 1, which applies for aircraft B pursuing A.

If the loft-ceiling-match curve forms part of the boundary of the capture set, as in Fig. 6 of Ref. 1 (A pursuing B), the energy multiplier final values for capture along the loft-ceiling-match portion will be related by transversality. With h_{L_1} and h_{L_2} the loft-ceilings for evader and pursuer, respectively, the inequality

$$h_{L_{2_f}} - h_{L_{1_f}} \geq 0 \tag{1}$$

and the equation $\Delta\chi_f = 0$, together defining capture, may be treated formally by adjoining their left members to the criterion function, final time t_f, to form the augmented function

$$P = t_f + \Lambda_\chi \Delta\chi_f + \Lambda_{h_L}(h_{L_{2_f}} - h_{L_{1_f}}) \tag{2}$$

The usual transversality analysis leads to

$$H_f = -1 \tag{3}$$

$$\lambda_{\chi_f} = \Lambda_\chi \tag{4}$$

$$\lambda_{E_{1_f}} = -\Lambda_{h_L} \mathrm{d}h_{L_{1_f}}/\mathrm{d}E_1 \tag{5}$$

$$\lambda_{E_{2_f}} = \Lambda_{h_L} \mathrm{d}h_{L_{2_f}}/\mathrm{d}E_2 \tag{6}$$

Received Nov. 18, 1975; presented at the AIAA 3rd Atmospheric Flight Mechanics Conference, Arlington, Texas, June 7-9, 1976 (in bound volume of Conference papers, no paper number); revision, including addition of weapon-envelope material, received Nov. 5, 1976.

Index categories: Aircraft Performance; Military Aircraft Missions; Navigation, Control, and Guidance Theory.

*Vice President. Associate Fellow AIAA.

†Senior Programmer/Analyst.

Imposing these conditions at a selected terminal capture point on the loft-ceiling-match curve in energy space defines a one-parameter family of trajectory pairs, i.e., one of the two parameters Λ_χ and Λ_{h_L} is defined by Eq. (3), while the other can be regarded as the parameter of the family.

The limiting trajectory pairs corresponding to near-miss or grazing trajectories are of special interest and correspond to $H=0$. Such pairs are not proper members of the family but define the *barrier surface* which, when closed, separates successful evasion and successful pursuit. The special values of the ratio $\Lambda_\chi/\Lambda_{h_L}$ that make H vanish may be determined iteratively. There may be one, two, or more of such values, or none. Some insight into this is provided by the relationship between the dual hodograph figures introduced in Ref. 1. Such a figure is drawn for loft-ceiling-matched energies using $\dot{\chi}$ for the ordinate and $(dh_L/dE)\dot{E}$ for the abscissa. The number of intersections of the two hodograph figures in the upper quadrants equals the number of vanishings of H. If one figure lies entirely within the other, there are none; this means one aircraft is locally superior and that there are no grazing trajectories through the point. An intersection in the upper quadrants implies $h=0$ by the existence of a common tangent to the figures; a perpendicular to this through the origin defines the direction of the corresponding multiplier vector. The term "tangent" is employed loosely here to include contact at a corner of the figure.

Composite "Fast-Evader" Trajectories

If the pursuer does not have any kind of low-energy superiority, the trajectory pairs are unbroken (except for what might be called "ordinary" corners, those satisfying the Erdmann condition) and can be found by integration of Euler solutions backwards in time using final multiplier values determined from Eqs. (3-6); trajectories terminating at various points of the capture set's boundary computed in this way determine the barrier surface.

What might be called generalized corners, i.e., corners with multiplier jumps, appear when the pursuer is superior in maximum sustainable turn rate and at the same time inferior in maximum instantaneous turn rate along the matched-loft-ceiling curve in energy space. When the opposing aircraft have this relationship, the pursuer, even having attained near angular closure with sufficient energy, is unable to effect capture immediately but only manages to force the evader into a high-turn-rate maneuver and to steer the chase toward lower energies where capture may take place. It can be argued that sustainable-turn-rate-superiority of the pursuer along the matched-ceiling curve to the lowest energies permitting flight makes closure with matched-loft-ceiling energy tantamount to subsequent capture. The appearance of at least some such two-subarc trajectories is insured with less overwhelming superiority, i.e., superiority of pursuer in maximum sustainable turn rate with energies of both craft unrestricted; in this case, a segment of the matched-loft-ceiling curve will be the locus of generalized corner junctions. The upper end of this segment is defined by the limit of the pursuer's sustainable-turn-rate superiority. The lower end will be on or below the lower edge of the band of pursuer energies defined by pursuer sustainable turn rate superiority over the evader's highest sustainable turn rate determined with his energy unrestricted. The arguments needed to establish that closure with matched-loft-ceiling energy along this segment insures subsequent capture are elementary and similar to those employed for the sufficient condition of Ref. 1.

Attention is now directed to the generalized corner junction of extremals appearing in this case where the pursuer has superiority at low energy but lacks a margin of maximum instantaneous turn-rate to turn closure immediately into capture at high energy. Consider a family of Euler solutions through an initial point having $\Delta\chi>0$ and pursuer energy high enough that some of the family members intersect $\Delta\chi=0$ above the loft-ceiling-match curve. Call $T(E_1, E_2)$ the time-to-capture measured from arrival at $\Delta\chi=0$, and Δt (not necessarily small) the time elapsed during the motion along the first subarc. Then an augmented performance index may be set up as

$$P=T(\bar{E}_1, \bar{E}_2)+\Delta t+\nu(\bar{h}_{L_2}-\bar{h}_{L_1})+\bar{\Lambda}_\chi\bar{\Delta\chi} \tag{7}$$

where the superscribed bars denote values at arrival at the surface $\Delta\chi=0$. If the inequality

$$\bar{h}_{L_2}-\bar{h}_{L_1}\geq 0 \tag{8}$$

is met with a margin, then $\mu=0$. The equality will obtain in many cases, however, since the pursuer will generally tend to sacrifice energy margin for turn-rate in effecting closure.

A transversality analysis carried out with the inequality (8) and $\Delta\chi=0$ regarded as an intermediate target set leads to the system

$$\bar{H}=-1 \tag{9}$$

$$\bar{\lambda}_\chi=\bar{\Lambda}_\chi \tag{10}$$

$$\bar{\lambda}_{E_1}=\frac{\partial T}{\partial \bar{E}_1}-\nu\frac{dh_{L_1}}{dE_1} \tag{11}$$

$$\bar{\lambda}_{E_2}=\frac{\partial T}{\partial \bar{E}_2}+\nu\frac{dh_{L_2}}{dE_2} \tag{12}$$

For extremal subarcs entering the surface $\Delta\chi=0$ with strict inequality ($>$) in (8), $\nu=0$ and the conditions (9-12) determine all of the multipliers. For $\nu\neq 0$, there is a one-parameter family whose limiting members occur for ν unbounded; these are not proper members, as $\bar{H}=0$. The ratio of multipliers

$$\bar{\lambda}_{E_1}/\bar{\lambda}_{E_2}=\frac{dh_{L_1}}{dE_1}\Big/\frac{dh_{L_2}}{dE_2} \tag{13}$$

is well defined in the limit. These multipliers and λ_χ are defined only within a multiplicative constant for these grazing trajectories. (Note that this corresponds to the classical definition of abnormality in variational problems: nonuniqueness of the multipliers.)

The generalized corner condition of Bernhard[3] furnishes a guide to which components of the multiplier vector jump and which do not, viz. the jump is normal to the singular surface. For $\nu=0$, this surface is the portion of the plane $\Delta\chi=0$ above the matched-loft-ceiling curve, and only the multiplier λ_χ jumps. For $\nu\neq 0$, it is the boundary defined by the equality sign in (8), and the energy multipliers jump to their values $\partial T/\partial E_1$ and $\partial T/\partial E_2$ from the values (11) and (12); there is no jump in the component of the energy-multiplier vector along the loft-ceiling-match curve's tangent.

Constructing nongrazing trajectory pairs that have two subarcs and terminate in capture from the first-order necessary conditions is fairly laborious. First, "open-loop" trajectory pairs connecting the capture set and the intermediate target set defined by (8) and $\Delta\chi=0$ are obtained. These are the second subarcs of composites and their energy multipliers provide the partials $\partial T/\partial E_1$ and $\partial T/\partial E_2$ needed in (11) and (12). The system (9-12) then provides multiplier end conditions for backward integration of Euler solutions which are the appropriately matched first subarcs.

A stroke of good fortune is that grazing trajectory pairs, of main interest because they define the barrier, are relatively easy to calculate. This limiting case has the first-subarc terminal values independent of the second-subarc solution; the partials $\partial T/\partial E_1$ and $\partial T/\partial E_2$ do not appear in Eq. (13), which greatly simplifies the calculation of the barrier surfaces. A similar situation occurs with the neutral-evader model, to be taken up next.

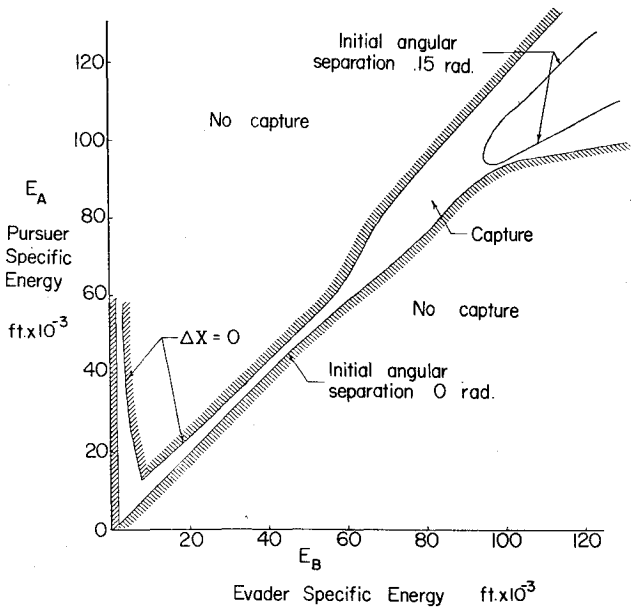

Fig. 1 Barrier surface – pursuer/evader = A/B.

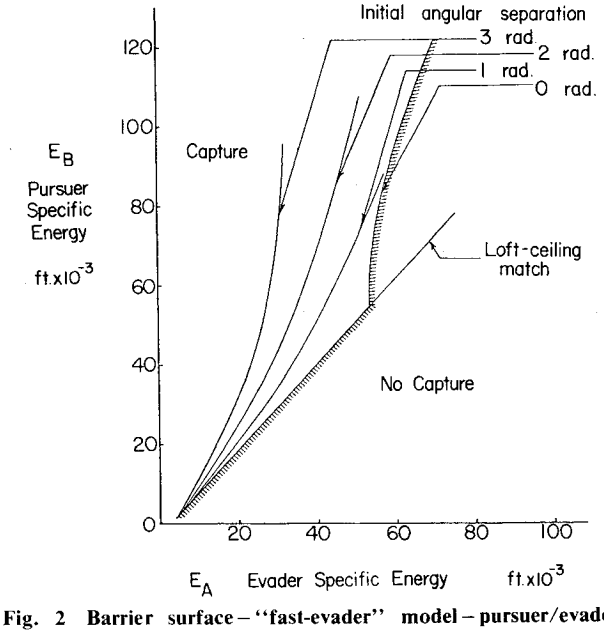

Fig. 2 Barrier surface – "fast-evader" model – pursuer/evader = B/A.

"Neutral-Evader" Model

Adoption of the more realistic "neutral-evader" model leads to families of solutions having a more complex structure, as discussed in Ref. 2. Under circumstances somewhat similar to those in which two-subarc solutions arise with the simpler model, solutions having a third, middle, subarc of so-called "tandem motion" appear. The tandem motion may itself be complex, including the singular arcs discussed in Ref. 2. The discussion of this section will ignore the possible appearance of singular subarcs, whose role is not fully understood at present. It is worth noting, however, that all of the singular subarcs found computationally in the examples to date have been screened out by one test or another, hence the assumed nonappearance may not be unduly restrictive.

Trajectories of "tandem-loft" type, calculated by the procedure and computer program described in Ref. 4, are shown in energy space in Fig. 3 for aircraft B as pursuer and A as evader. There is one trajectory of particular interest that bifurcates, dividing the family. Those above it generally

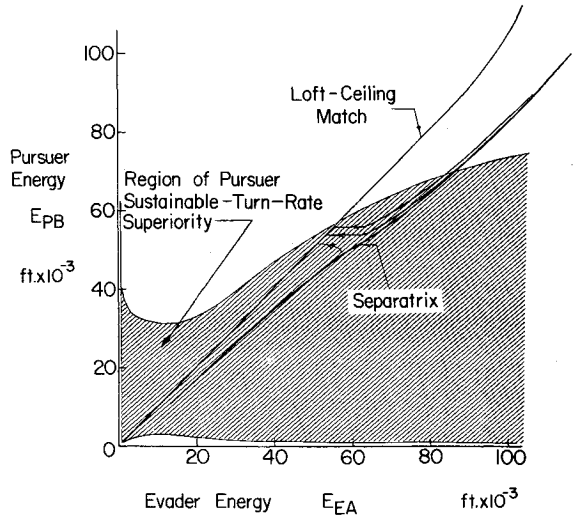

Fig. 3 Tandem/loft trajectories and separatrix.

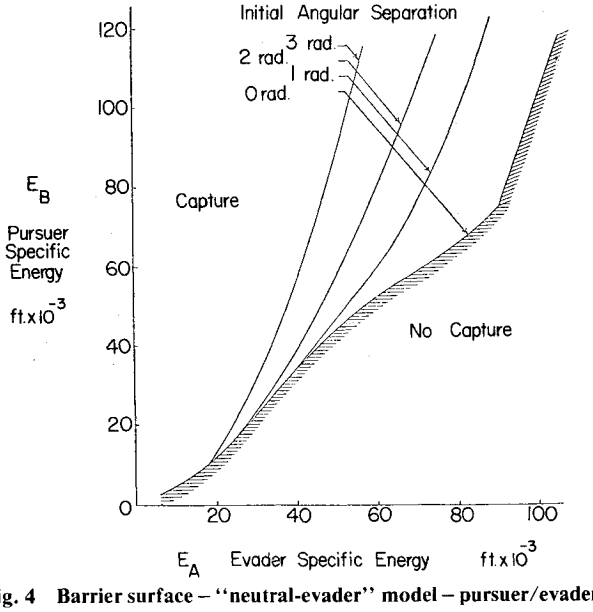

Fig. 4 Barrier surface – "neutral-evader" model – pursuer/evader = B/A.

produce a loss of pursuer energy and originate at high pursuer energies. Those below the bifurcating trajectory correspond generally to increasing pursuer energy (although not monotonically), and originate at low pursuer energies. The two branches of the bifurcating trajectory form a *separatrix*, a boundary outside of which the tandem-loft motion does not attain loft-ceiling match.

The family of tandem/loft trajectories is determined by numerical integration using a computer program such as that described in Ref. 4. As a preliminary, loft-ceiling rates at matched-loft-ceiling altitudes may be compared at various points along the loft-ceiling-match curve in energy space, as in Fig. 5 of Ref. 2. This was carried out with the computer program of Ref. 5, which also performs a single step of integration backwards in time using a coarse integration technique (Euler extrapolation) to assist the search for the bifurcating trajectory and the separatrix.

The region in energy space between the separatrix and the loft-ceiling-match curve plays a role in the neutral-evader trajectory family analogous to that of the loft-ceiling-match curve in that of the simpler fast-evader model. Trajectory pairs corresponding to pursuer closure with insufficient energy undergo transitions in this region to tandem-loft motion, which may continue until the loft-ceiling-match curve

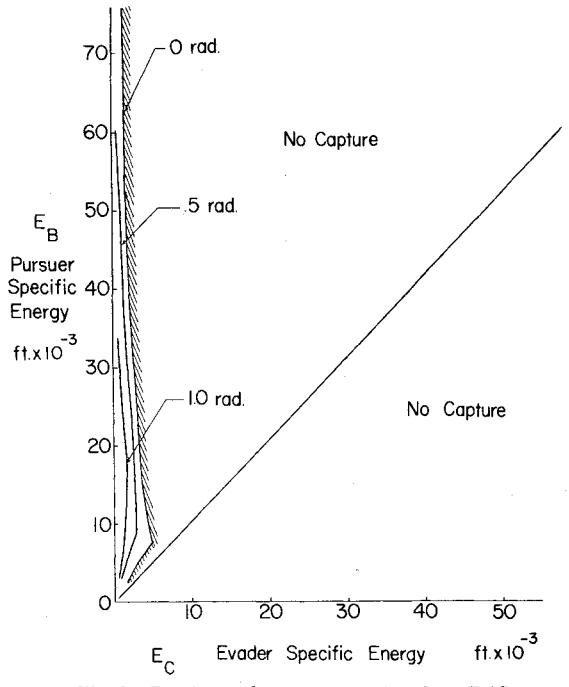

Fig. 5 Barrier surface – pursuer/evader = B/C.

is reached; then either capture occurs or a transition to a high-turn-rate open-loop-optimal pair. The grazing trajectories for $H=0$ join with tandem-loft arcs on the separatrix when the hodograph figures are in the proper relationship, previously described; however, the scaling factors on the energy-rate axes of these figures are different: they are the magnitudes of the energy multipliers. The ratio of these is of main importance, and, along the separatrix, this ratio for $H=0$ is obtained as

$$\left| \frac{\lambda_{E_2}}{\lambda_{E_1}} \right| = \left| \frac{\dot{E}_1}{\dot{E}_2} \right| \tag{14}$$

This may be viewed as the determination of the normal to a two-dimensional trajectory from the components of velocity. The relationship (14) is employed like Eq. (13) in the determination of multipliers from transversality conditions generally similar to those given for the fast-evader model. The computation of barrier candidates comes down to the use of Eq. (14) for the energy-multiplier ratio together with $H=0$ solved iteratively for the ratio of λ_χ to one of the energy multipliers.

The segment of the separatrix which is the locus of generalized corners for barrier trajectory pairs is simply related to the corresponding segment of the loft-ceiling-match curve discussed previously for the fast-evader model. The relating property is that tandem-loft trajectory pairs originating on the separatrix segment must remain within a region in energy space characterized by the existence of at least one dual-hodograph-figure intersection and reach the matched-loft-ceiling curve, otherwise a transition to 3-D motion and successful evasion is possible. The argument is similar to that for the sufficient condition of Ref. 1. In the example of aircraft B chasing A, the entire separatrix maps into a single point on the loft-ceiling-match curve which is within the region of pursuer-superior sustainable turn rate (shaded in Fig. 3) and hence well within the intersecting-dual-hodograph region.

It appears possible that the locus of generalized corners of barrier trajectories in energy space may sometimes be a composite including segments of the separatrix, the boundary of the intersecting-dual-hodograph region between the separatrix and the loft-ceiling-match curve, and the loft-ceiling-match curve itself. Along the intersecting-dual-hodograph boundary, the multiplier ratio analogous to Eqs. (13) and (14) may be obtained from the normal to the boundary.

Computation of Barrier Surfaces

Families of trajectory pairs integrated backwards in time numerically define the barrier surfaces. All start at $\Delta\chi=0$ and at pairs of specific energies along the types of curves in the energy space previously discussed. Multiplier values are determined as discussed in the preceding sections. The present section discusses the procedure and sequence of calculations employed with computer programs such as those of Refs. 4 and 5.

Perform first a comparison of energy rates and sustainable turn rates with energies matched over the energy range for equal loft-ceilings. The computation of the barrier surface for the sustainable-turn-rate-superior aircraft as *evader* proceeds entirely from the boundary of the capture region. If this lies completely above the loft-ceiling-match curve, the boundary is defined by matching of maximum instantaneous-turn-rates; if not, some portion of the loft-ceiling-match curve itself may form a portion of the boundary. The energy multiplier end values are zero for maximum-instantaneous-turn-rate match and given by Eq. (13) for loft-ceiling match. The value of λ_χ is found in the latter case from $H=0$. The program of Ref. 4 does this by a scan followed by an iteration. If two values of λ_χ emerge from this computation, one of them may be of interest when the aircraft pursuer/evader roles are reversed.

For the sustainable-turn-rate-superior craft as *pursuer,* segments of the loft-ceiling-match curve, the separatrix, and the sustainable-turn-rate boundary may form part of the locus of generalized corners of barrier trajectories. If there is a region of tandem/loft motion that leads to loft-ceiling match, the separatrix should be found, then a composite locus of generalized corners for barrier trajectories by examining the tandem-loft trajectory family relative to the sustainable-turn-rate-superiority region of the pursuer.

Computational Results for A vs B

Some results are presented in Figs. 1, 2, and 4 of barrier surfaces for turning duels between aircraft A, a hypothetical Mach 3 design, and aircraft B, a version of the F-4 used for illustrative computations in Refs. 1 and 2.

Figure 1 applies for A chasing B; it is the same for both fast-evader and neutral-evader models. The upper boundary of the capture set is the instantaneous-turn-rate-match curve, while the lower is the loft-ceiling-match curve. Integrations of trajectory pairs never develop appreciable positive $\Delta\chi$ values except at high energies; even in the region most favorable to A, only small angle differences can be closed successfully.

Figure 2 is for fast-evader modeling, B chasing A. The trajectory pairs defining the barrier all pass through the lower portion of the loft-ceiling-match curve.

Figure 3 shows the region of tandem motion for B chasing A and the separatrix arising from bifurcation of a tandem/loft trajectory that divides the region. All of the tandem trajectories considered are of tandem/loft type, since all chattering singular arc segments are screened out by failure to meet one requirement or another.[2] The pursuer-sustainable-turn-rate region is shown shaded.

Figure 4 shows the barrier surface for B chasing A, neutral-evader modeling. The trajectory pairs defining the barrier pass through the separatrix, only a small upper portion of the separatrix proving barren. The difference between the barrier results for fast-evader and neutral-evader models is large in this example and implies that the tandem/loft pursuit tactic is important. It should be noted that this may be untypical because of an anomaly in the otherwise realistic data for aircraft A: $C_{L_{max}}$ was taken as unity independent of Mach number; this is an especially optimistic figure supersonically. This leads to an energy-rate advantage for B when both craft fly at matched-loft-ceiling altitude, hence favors the lofting tactic for B as pursuer.

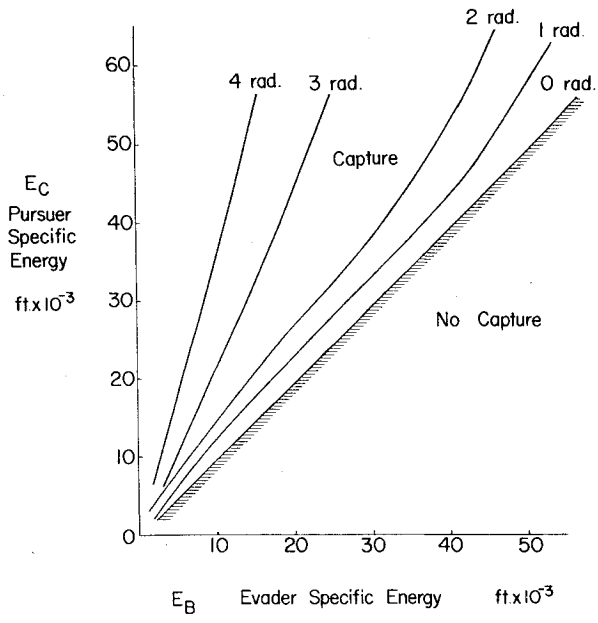

Fig. 6 Barrier surface – pursuer/evader = C/B.

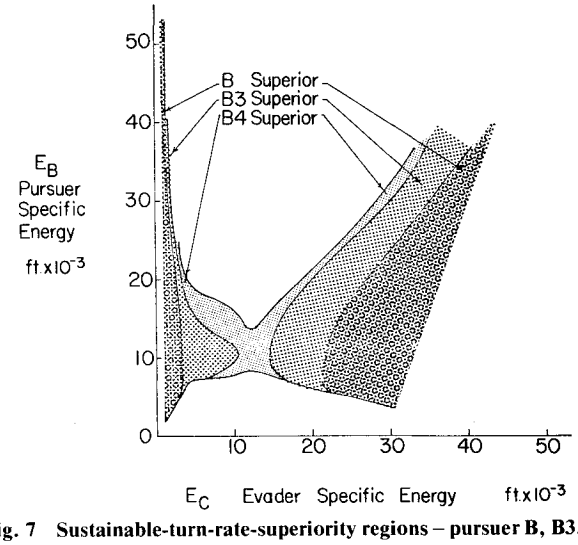

Fig. 7 Sustainable-turn-rate-superiority regions – pursuer B, B3, B4; evader C.

Results for B vs C with Parameterized Thrust

Shown next are some results for aircraft B (F-4) against C, a version of the F-5. B can reach substantially higher energies than C (110 K vs 70 K); however, it is inferior to C in both maximum sustainable turn rate and maximum instantaneous turn rate at matched loft-ceilings. The mismatch in capabilities between B and C resembles somewhat the mismatch seen in the preceding example between A and B, but is not as extreme. The trajectory families are simpler in two respects: the opportunities for successful tandem-lofting pursuit are negligible (and have been omitted entirely in the computations), and the relationship between maximum instantaneous turn rates is such that high-turn-rate spirals to low energy occur only for B chasing C, i.e., C can capture at high energy. Taken together, these characteristics result in simple pairing of trajectories in all cases; there are no multiple-subarc trajectories in the families.

Figure 5 presents barrier-surface results for B pursuer and C evader. Successful pursuit occurs only for C in the low energy range and for B with a large initial energy advantage in combination with an angular position advantage.

Figure 6 shows barrier data for C chasing B. Generally, an energy advantage is needed by C to capture B before the chase

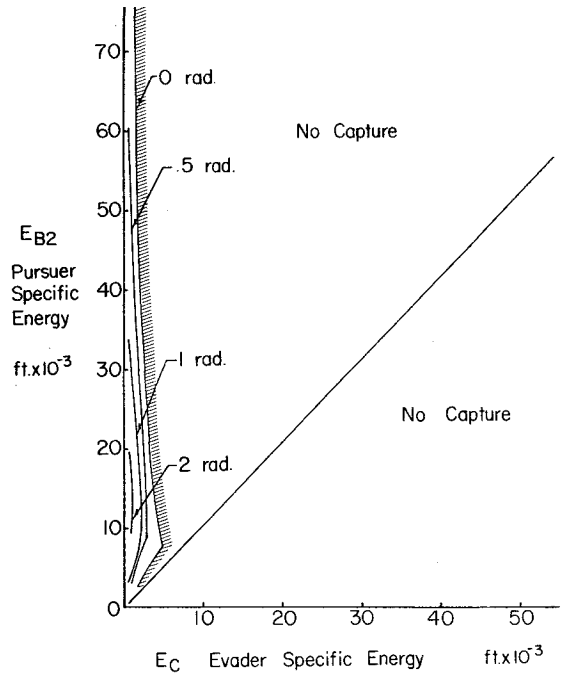

Fig. 8 Barrier surface – pursuer/evader = B2/C.

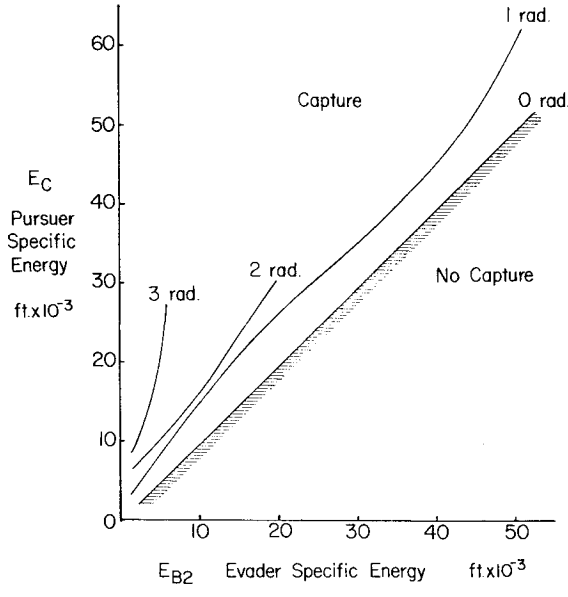

Fig. 9 Barrier surface – pursuer/evader = C/B2.

reaches B's high-energy haven. Given such an advantage, C can close fairly large angular gaps and capture when the initial energies are low; however, at high initial energies, only modest closures can be effected even with large energy advantage.

A computational study of barrier behavior as B's thrust level is increased was carried out. An important guide to the behavior is provided by the sustainable-turn-rate boundaries in energy space depicted in Fig. 7. Configuration B2 has 20% thrust increase over the basic value over the entire Mach number/altitude range, B3 30%, B4 40%. The situation is similar to that of the B/A example as in Fig. 3, although simpler in respect to the absence of tandem/loft motion. As the thrust is increased from 30% to 40% over basic, B develops an overall superiority in maximum sustainable turn rate, energy choice open, and the barrier surface for B pursuing C disappears, implying eventual capture in a long-duration chase irrespective of initial conditions. Barrier surfaces in Figs. 8, 9, and 10 show the shifts in capture

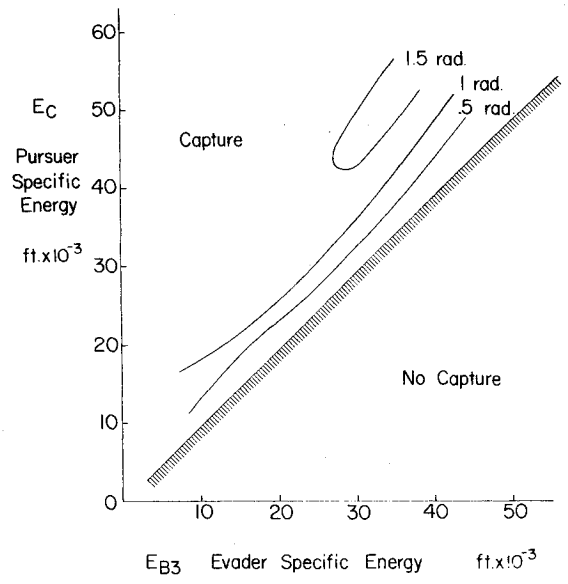

Fig. 10 Barrier surface – pursuer/evader = C/B3.

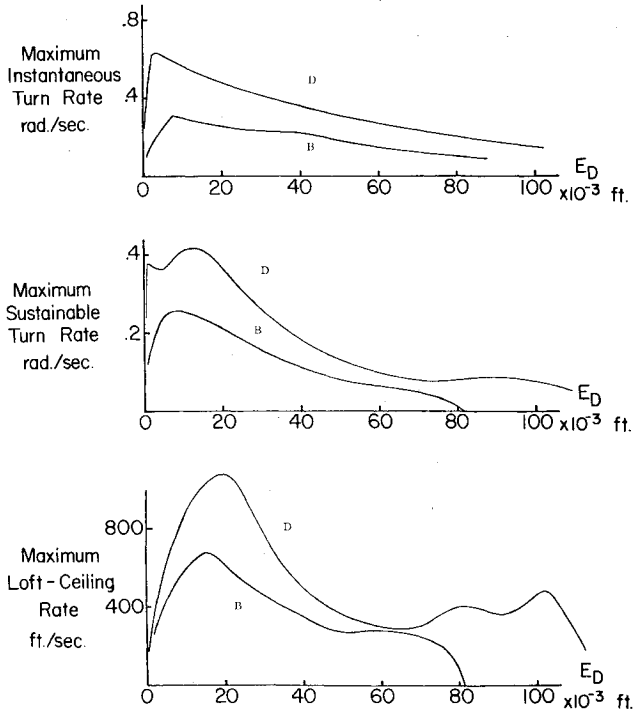

Fig. 11 Hodograph comparison at matched loft-ceiling energies – configurations B and D.

capability as B's thrust is increased. The results shown are only rough approximations on account of coarseness of mesh of the trajectory data.

Results for a Trapezoidal-Wing RPV Configuration

Some calculations were carried out for the high-performance RPV configuration of Ref. 6. Maximum instantaneous turn rate, maximum sustainable turn rate, and maximum loft-ceiling rate vs energy are shown for this configuration, designated D, in Fig. 11, where the corresponding characteristics of aircraft B are also shown for comparison. The superiority of D over B is overwhelming; the sufficient condition of Ref. 1 is met and eventual capture in role-determined D/B engagements is insured irrespective of initial conditions.

A similar comparison of hodograph data for D and A is shown in Fig. 12. D is seen to be superior in the dogfighting

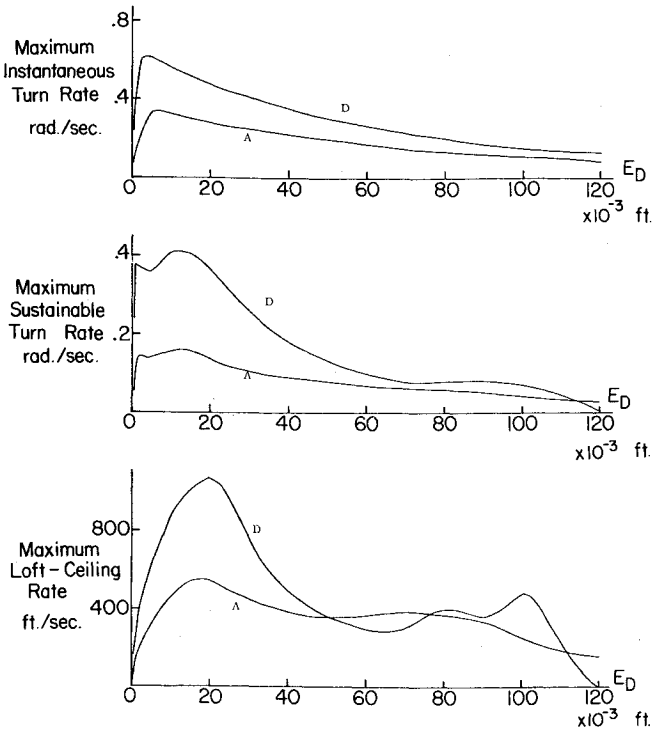

Fig. 12 Hodograph comparison at matched loft-ceiling energies – configurations A and D.

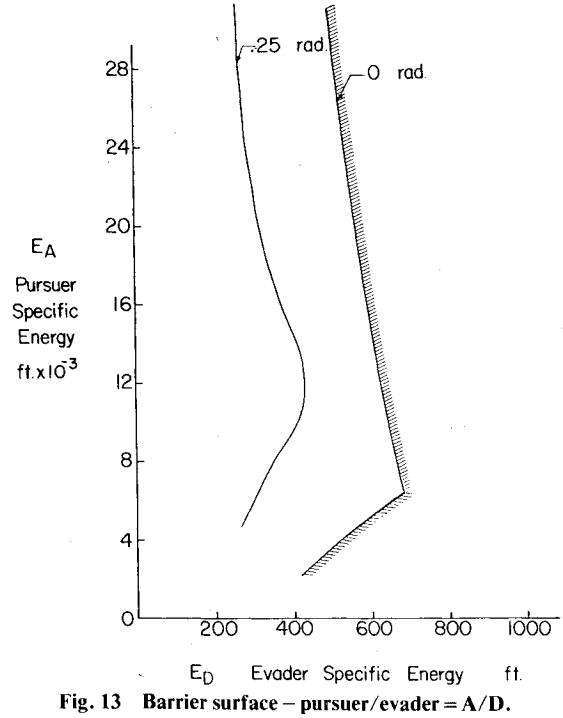

Fig. 13 Barrier surface – pursuer/evader = A/D.

energy range; the superiority wanes above 100K energy because of inlet off-design characteristics. The barrier results of Fig. 13 show A incapable of capture except at extremely low evader energy and then only with tremendous energy and angular position advantages. The barrier surface of Fig. 14 indicates high effectiveness of D pursuing A except at high energies near A's haven. Fragmentary trajectory data in the energy range 60-100K indicate that the poorly-defined barrier surface may actually fold over into the region below the loft-ceiling-match curve (marked *"No Capture"*) for large angular separation; there is some difficulty in representing the surface graphically here, in addition to a coarseness-of-mesh problem.

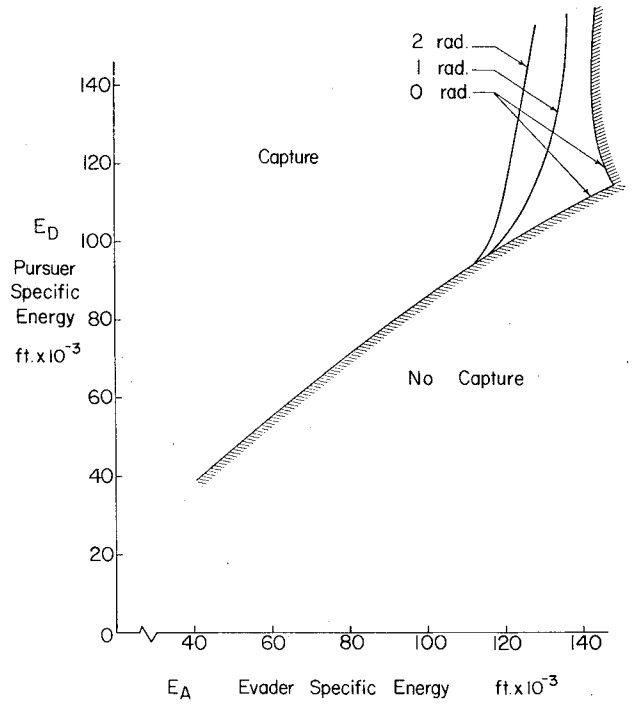

Fig. 14 Barrier surface – pursuer/evader = D/A.

Weapon Capture

As in Refs. 1 and 2, the state of each vehicle is expressed in energy approximation by a specific energy $E \equiv h + (V^2/2g)$ and a turn or heading angle χ, measured from a reference direction in the horizontal plane. Since only the difference $\Delta\chi = \chi_1 - \chi_2$ is of interest, the state vector of the differential-turning game is E_1, E_2, $\Delta\chi$. The extended capture criteria accounting for weaponry are

$$|\Delta\chi| \leq \sigma \tag{15}$$

$$h_{L_2} + m \geq h_{L_1} \tag{16}$$

where σ is the weapon's conical trainability limit half-angle and m is the vertical component of the reach of a weapon of lethal radius r.

$$m = r\sqrt{\sin^2\sigma - \sin^2\Delta\chi} \leq r\sin\sigma \tag{17}$$

as in Fig. 15.

It should be noted that for $\sigma = 0$ and $r = 0$, the criteria reduce to matching turn angle and equalling or exceeding evader's loft-ceiling.

"Fast-Evader" Computational Procedure with Weapon-Capture

The simpler of the two models studied in Ref. 2, termed "fast evader," is first examined. It is the less realistic of the two, occasionally adequate with well-matched opponents in gun duels but badly lacking with weaponry having appreciable upward reach; thus it is included mainly for completeness. The usual transversality analysis at terminal capture leads to

$$\lambda_{E_{1_f}} = -\lambda_{h_L} \frac{dh_{L_{1_f}}}{dE_{1_f}} \tag{18}$$

$$\lambda_{E_{2_f}} = \lambda_{h_L} \frac{dh_{L_{2_f}}}{dE_{2_f}} \tag{19}$$

$$\lambda_{\chi_f} = \Lambda_\chi + \Lambda_{h_L} \frac{dm}{d\Delta\chi_f} \tag{20}$$

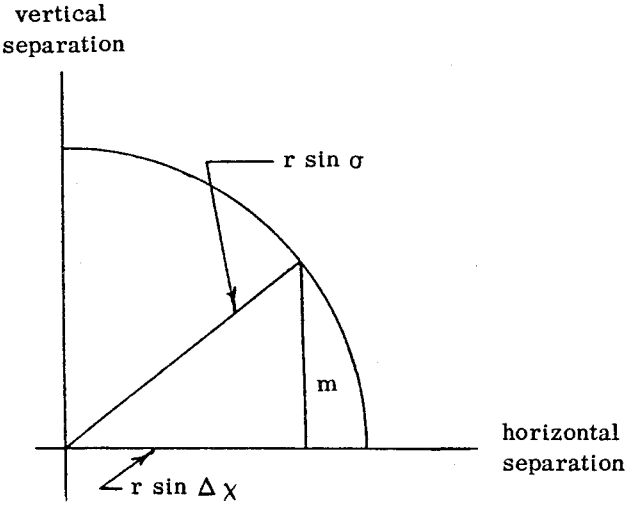

Fig. 15 Sketch.

where Λ_χ and Λ_{h_L} are constant multiplier variables used to adjoin Eqs. (15) and (16). If the strict inequality in (15) is satisfied, $\Lambda_\chi = 0$; similarly, $\Lambda_{h_L} = 0$ if the pursuer has a surplus of energy at capture. Both vanish only in the special case of initial capture.

Preliminary "hodograph" computations are first performed; however, they are more extensive than usual. A sequence of points in E_1, E_2 space defining loft-ceiling match are computed and, at each of these, comparative values of maximum instantaneous turn rate, maximum sustainable turn rate, and loft-ceiling rate $\dot{h}_L = (dh_L/dE)\dot{E}$ are calculated; this applies for one extreme of marginal capture, viz. $|\Delta\chi| = \sigma$. For the other, $\Delta\chi = 0$, the appropriate energy matching is "offset matching," $h_{L_2} + r\sin\sigma = h_{L_1}$, and similar rate comparison computations are carried out for this case. If the pursuer's energy exceeds the loft-ceiling-match value, capture does not have the near-miss character, $\lambda_{E_{1_f}} = \lambda_{E_{2_f}} = 0$, and the trajectory-pair is interior to any barrier surface.

Determination of final values for a backward integration from capture proceeds as follows. The evader's specific energy is fixed at a selected value; the pursuer's is at least the offset-match value, and, if the transversality conditions Eq. (18-20) are to apply with $\Lambda_{h_L} \neq 0$, it will not exceed the loft-ceiling-match energy. Within this range of pursuer energy, it may be assumed without loss of generality that $\Lambda_\chi = 0$ and $\Lambda_{h_L} = 1$, the latter to be rescaled eventually to satisfy $H = -1$. In the case of grazing trajectory pairs defining barrier surfaces of central interest, $H = 0$, and even this rescaling is unnecessary. Barrier candidates are sought by adjusting pursuer energy such that $H = 0$, ordinarily by a coarse scan followed by an iteration to pinpoint the zero. Should no zero be found, the remaining possibility is $\Delta\chi = \sigma$, $\Lambda_\chi \neq 0$, and pursuer energy equal to the loft-ceiling-match value. This is explored by varying the ratio $\Lambda_{h_L}/\Lambda_\chi$ to obtain $H = 0$ by scan and iteration in the same manner as for the case of zero weapon lethal radius, $r = 0$ discussed earlier. The control variables are determined through the course of the searches by minimax of H. Under circumstances similar to those described earlier for point capture, the preceding applies also to conditions at a "generalized corner" at an intermediate target point.

"Neutral-Evader" Computational Procedure with Weapon-Capture

The 2-D "tandem-loft" motion described in Ref. 2 must be calculated with $\Delta\chi = 0$ and the altitudes h_2 and h_1 of pursuer and evader subject to

$$h_2 + m \geq h_1 \tag{21}$$

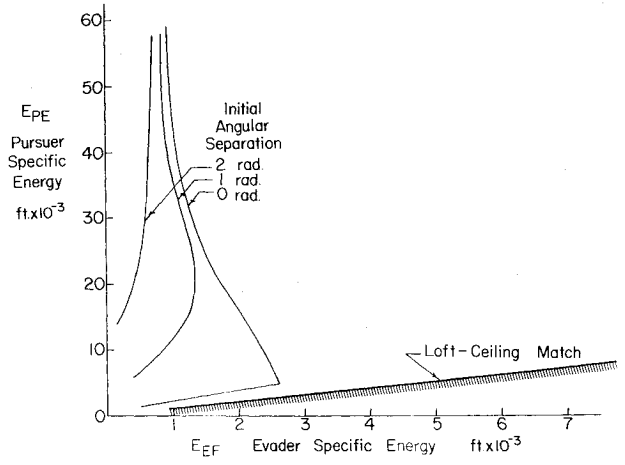

Fig. 16 Barrier surface – point capture – pursuer/evader = E/F.

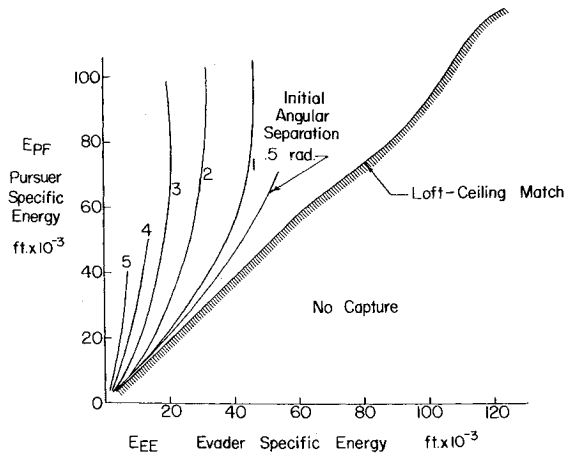

Fig. 18 Barrier surface – point capture – pursuer/evader = F/E.

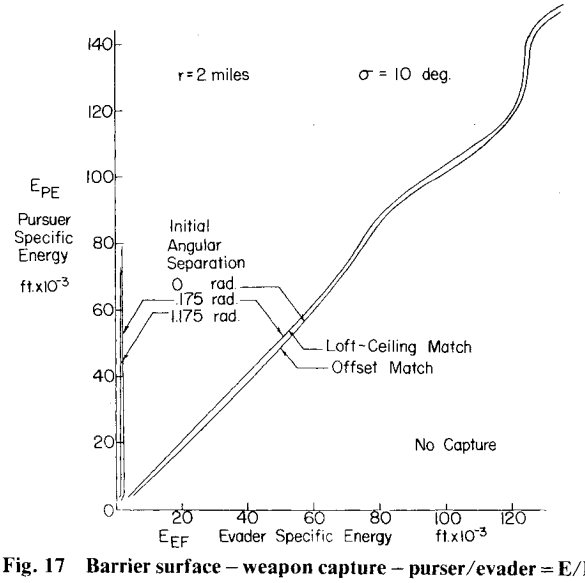

Fig. 17 Barrier surface – weapon capture – purser/evader = E/F.

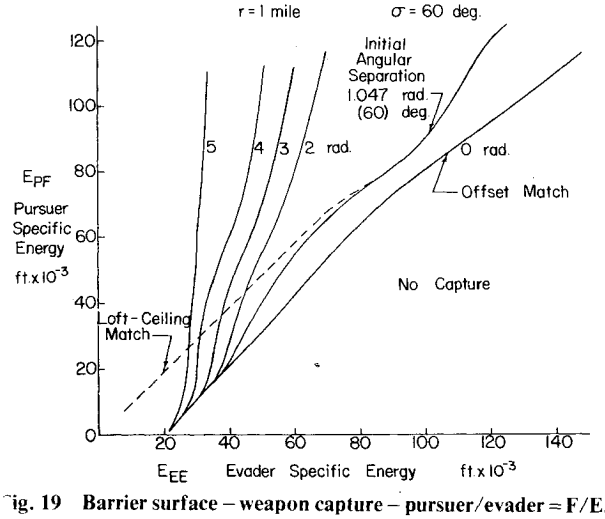

Fig. 19 Barrier surface – weapon capture – pursuer/evader = F/E.

over a range of values of m. The controls h_2 and h_1 are determined by minimax of H subject to Eq. (21).

$$H = H_1 - H_2 = \lambda_{E_1}\dot{E}_1 + \lambda_{E_2}\dot{E}_2 \tag{22}$$

The specific energies and the variables λ_{E_1} and λ_{E_2} are calculated by backward numerical integration of state and adjoint systems with

$$\lambda_{E_{1_f}} = \mathrm{d}h_{L_{1_f}}/\mathrm{d}E_{1_f} \tag{23}$$

$$\lambda_{E_{2_f}} = -\mathrm{d}h_{L_{2_f}}/\mathrm{d}E_{2_f} \tag{24}$$

The computation of a family and its separatrix must be carried out for $m=0$, $m=r\sin\sigma$, and for intermediate values, unless linear interpolation between the extremes is to be employed as an approximate representation, which is often reasonable.

Whatever approximation is chosen, the energy-matching requirement for capture is expressed as

$$E_2 - E_2'(E_1, m) \geq 0 \tag{25}$$

where the function E_2' is represented as, say, a spline-lattice, or by linear interpolation between cubic spline representations of separatrices.

The terminal values of multiplier variables for backward numerical integration of 3-D trajectory pairs are given by

$$\lambda_{E_{2_f}} = 1 \tag{26}$$

$$\lambda_{E_{1_f}} = -\frac{\partial E_2'}{\partial E_1} \tag{27}$$

$$\lambda_{\chi_f} = \frac{\partial E_2'}{\partial m}\frac{\sin\Delta\chi_f \cos\Delta\chi_f}{\sqrt{\sin^2\sigma - \sin^2\Delta\chi_f}} \tag{28}$$

Barrier-trajectory pair candidates are found by searching vs pursuer energy, with evader energy fixed, for $H=0$ in a scan and iteration process similar to that mentioned earlier for the simpler "fast-evader" model. If no zero is found, pursuer energy is fixed at the separatrix value E_2' for $m=0$, the λ_E multipliers at the values given by Eqs. (26) and (27), and λ_χ varied to obtain $H=0$ as in point capture.

Weapon-Capture Computational Results

Barrier surface results will be presented for duels between two fighter aircraft of hypothetical, but realistic, design by NASA-Ames' Aeronautical Systems Division. Aircraft E's design favors supersonic climb, cruise, and maneuvering; its weapons are conventional missiles represented in rough approximation by an envelope having a conical half-angle of 10° and a lethal radius limit of 2 statute miles. Aircraft F's design is more conventional in favoring subsonic and transonic characteristics but it is configured for special weaponry, $\sigma = 60°$ and $r = 1$ statute mile.

The barrier surface for E pursuing F under point-capture rules is shown in Fig. 16. Because the pursuer does not enjoy an advantage in either maximum instantaneous or maximum sustainable turn rate at loft-ceiling-match energies, he can capture only at low evader energies, and then only with a substantial energy advantage. The use of weaponry furnishing 10° half-angle and 2-mile reach permits capture at high energies as shown in Fig. 17; however, it is limited to initial capture except in essentially the same low-evader-energy region as for point capture.

Figure 18 presents the point-capture barrier surface for F pursuing E. Capture can be effected with large initial angular gaps at low energies with a pursuer energy advantage. Nonetheless, a composite win-lose-draw region for point-capture duels between E and F shows a very large draw region.

Figure 19 presents the weapon-capture barrier surface for F pursuing E with $\sigma = 60°$, $r = 1$ mile weaponry. The increase in F's win region in the joint state space is seen to be large. This is mainly attributable to the upward reach of the weapon $m = r \sin\sigma$, although the effect of improved angular coverage is substantial.

Perhaps the most interesting lesson from these computations is that a large draw region in the joint state space still remains, even though the upward reach of F's weaponry is only about 2000 ft short of that needed for transition to an open barrier surface which would signify eventual capture of E by F irrespective of initial conditions. In simpler terms, the difference between the absolute ceilings of F and E exceeds $r \sin\sigma$ only slightly; thus E's high-energy haven is almost sealed off, and one would expect few draws, yet E manages to exploit his remaining haven remarkably well. Near-superiority is not enough – small margins, negative or positive, make large differences.

Concluding Remarks

A procedure has been presented for the calculation of barrier surfaces for differential-turning duels and examples given. Three computer programs, each fairly complex, were used and a certain amount of crossplotting of intermediate data was required in the first computational example; however, considerable streamlining of the programs and computations was carried out in the process of the subsequent applications and the generation of barrier surface data can be regarded as a practical proposition for engineering applications work.

Upward reach appears to be the main effect of weaponry in the differential-turn model, with angular trainability of some consequence. Extended-envelope weaponry can more easily overcome a gap in high-energy performance and ceiling than it can a deficiency in turn rate in the "dog fighting" portion of the envelope: low altitude and subsonic/transonic speeds. Design tradeoffs should reflect this. Probably the differential-turn model underestimates the value of weapon reach sideways, as it is limited to roughly concentric circling motions of the opposing craft; this is not a severe limitation in study of turning duels with guns, but it tends to become severe for a weapon that cuts a wide swath through the sky.

Acknowledgment

This work was supported by Aeronautical Systems Division, NASA Ames Research Center, Moffett Field, Calif., under Contract NAS 2-8738.

References

[1]Kelley, H.J., "Differential-Turning Optimality Criteria," *Journal of Aircraft,* Vol. 12, Jan. 1975, pp. 41-44.

[2]Kelley, H.J., "Differential-Turning Tactics," *Journal of Aircraft,* Vol. 12, Dec. 1975, pp. 930-935.

[3]Bernhard, P., "Corner Conditions for Differential Games," Fifth IFAC Congress, Paris, France, June 12-17, 1972.

[4]Lefton, L., Krenkel, A.R., and Kelley, H.J., "A User's Guide to the Aircraft Energy-Turn and Tandem Motion Computer Programs," Analytical Mechanics Associates, Inc., Jericho, N.Y., Report No. 75-26, June 1975; revised edition, Jan. 1976.

[5]Lefton, L. and Kelley, H.J., "A User's Guide to the Aircraft Energy-Turn Hodograph Program," Analytical Mechanics Associates, Inc., Jericho, N.Y., Report No. 75-7, March 1975; revised edition, Jan. 1976.

[6]Nelms, W.P. and Axelson, J.A., "Preliminary Performance Estimates of a Highly Maneuverable Remotely Piloted Vehicle," NASA TN D-7551, Feb. 1974.